Odin observations of Antarctic nighttime NO densities in the mesosphere–lower thermosphere and observations of a lower NO layer

P. E. Sheese,[1] K. Strong,[1] R. L. Gattinger,[2] E. J. Llewellyn,[2] J. Urban,[3] C. D. Boone,[4] and A. K. Smith[5]

Received 14 November 2012; revised 4 June 2013; accepted 5 June 2013; published 11 July 2013.

[1] The Optical Spectrograph and Infrared Imaging System (OSIRIS) on the Odin satellite currently has an eight-year dataset of nighttime Antarctic nitric oxide densities, [NO], in the mesosphere–lower thermosphere (MLT) region. In this work, the OSIRIS data are compared with a similar data set from the Sub-Millimeter Radiometer (SMR), also on the Odin satellite. Both of the Odin data sets are compared with twilight [NO] from the Atmospheric Chemistry Experiment–Fourier Transform Spectrometer (ACE-FTS) on the SciSat-I satellite. Direct comparisons of OSIRIS and SMR profiles show large differences, indicating that the individual [NO] profiles of one or both data sets may not be valid. However, when comparing averaged [NO], variations on timescales of weeks-years in all three data sets are in good agreement and correspond to the 27 day and 11 year solar cycles. The averaged OSIRIS values are typically 10% greater than SMR and 30% greater than ACE-FTS, which are within the estimated OSIRIS systematic uncertainties. These results suggest that the satellite-derived data sets can be used for determining polar-mean NO climatology and variations on timescales of weeks-years. The OSIRIS and SMR nighttime data sets show that the [NO] peak height in the MLT decreases throughout the autumn, from an altitude near or above 100 km to a minimum altitude ranging from 90 to 95 km around winter solstice. A similar decrease in [NO] peak height is observed in modeled NO climatology from the Specified Dynamics–Whole Atmosphere Community Climate Model (SD-WACCM), although the SD-WACCM climatology exhibits a decrease throughout autumn from 107 km down to 102 km. The results suggest that global climate models require more sophisticated auroral forcing simulations in order to reproduce observed NO variations in this region.

Citation: Sheese, P. E., K. Strong, R. L. Gattinger, E. J. Llewellyn, J. Urban, C. D. Boone, and A. K. Smith (2013), Odin observations of Antarctic nighttime NO densities in the mesosphere–lower thermosphere and observations of a lower NO layer, *J. Geophys. Res. Atmos.*, *118*, 7414–7425, doi:10.1002/jgrd.50563.

1. Introduction

[2] Nitric oxide (NO) is an important trace species in the mesosphere–lower thermosphere (MLT) region. Not only do NO ionization and radiative cooling strongly influence the overall energy budget of the lower thermosphere, but both NO and NO_2 produced in the MLT region during the dark polar winter are transported down into the lower mesosphere and upper stratosphere, where they play a role in ozone destruction [*Solomon et al.*, 1982; *Funke et al.*, 2005a; *Randall et al.*, 2007]. However, satellite measurements of nighttime NO densities ([NO]) in the MLT are very limited.

[3] Over the past few decades, multiple satellite missions have measured [NO] and NO emission in the daytime MLT region. Observations of fluorescent emission in the NO gamma bands have commonly been used to derive [NO] profiles. This technique was first explored by *Barth* [1964] and used by the Solar Backscatter Ultraviolet (SBUV) spectral radiometer on board Nimbus-7 [*McPeters*, 1989], the Solar Mesosphere Explorer [*Barth et al.*, 1988], and the Student Nitric Oxide Experiment [*Solomon et al.*, 1999]. The Halogen Occultation Experiment (HALOE) on board the Upper Atmosphere Research Satellite derived [NO] from solar occultation measurements in the NO fundamental band at 5.26 μm [*Gordley et al.*, 1996]. The Atmospheric Chemistry Experiment-Fourier Transform Spectrometer (ACE-FTS) also currently retrieves [NO] from solar

[1]Department of Physics, University of Toronto, Toronto, Ontario, Canada.
[2]ISAS, Department of Physics and Engineering Physics, University of Saskatchewan, Saskatoon, Saskatchewan, Canada.
[3]Department of Earth and Space Sciences, Chalmers University of Technology, Göteborg, Sweden.
[4]Department of Chemistry, University of Waterloo, Waterloo, Ontario, Canada.
[5]Atmospheric Chemistry Division, National Center for Atmospheric Research, Boulder, Colorado, USA.

Corresponding author: P. E. Sheese, Department of Physics, University of Toronto, Toronto, ON M5S 1A7, Canada. (psheese@atmosp.physics.utoronto.ca)

2169-897X/13/10.1002/jgrd.50563

occultation measurements near the NO fundamental band [*Kerzenmacher et al*., 2008]. However, the measurements for each of these instruments are necessarily limited to daytime and twilight conditions.

[4] Both the Sounding of the Atmosphere using Broadband Radiometry (SABER) and the Michelson Interferometer for Passive Atmospheric Sounding (MIPAS) instruments, on board NASA's Thermosphere-Ionosphere-Mesosphere Energetics and Dynamics satellite and ESA's Environmental Satellite, respectively, observe NO fundamental band emission. In 2005, the MIPAS instrument began scanning above the nominal maximum observation tangent altitude of 68 km roughly one day out of 10, and *Funke et al*. [2005b] have described a [NO] retrieval technique for these scans. In contrast, SABER consistently scans from the stratosphere to the thermosphere, and its observations have been used to elucidate the role of NO emission in the MLT region energy budget [*Mlynczak et al*., 2003, 2005]. *Gardner et al*. [2007] discuss [NO($v=1$)] and [NO($v=0$)] retrievals from both SABER and MIPAS 5.3 μm emission observations and have shown that the [NO($v=0$)] retrievals in the MLT are highly sensitive to uncertainties in both the kinetic temperature and the atomic oxygen density profiles and require knowledge of atomic nitrogen concentrations in regions with auroral activity. *Bermejo-Pantaleón et al*. [2011] discussed MIPAS retrievals of NO concentrations both inside and outside of the auroral regions. However, the MIPAS results were limited to altitudes at and above 100 km, and nighttime NO concentrations were not explicitly discussed due to large smoothing errors.

[5] The Optical Spectrograph and Infrared Imaging System (OSIRIS) and the Sub-Millimeter Radiometer (SMR), both on board the Odin satellite, use two different observation techniques that yield nighttime retrievals of ground state [NO]. The SMR observes NO thermal emissions near 551.7 GHz, which are observable in both night and daytime conditions, and the OSIRIS retrieval makes use of measurements of the $NO + O\ (+M) \rightarrow NO_2\ (+M) + h\nu$ afterglow continuum (NO_2 continuum), which extends from 370 to 1400 nm, but is observable by OSIRIS only in nighttime visible spectra [*Gattinger et al*., 2009, 2010].

[6] The present study compares eight years (2003–2010) of the OSIRIS and SMR [NO] data sets for the dark Antarctic MLT and compares these data with ACE-FTS observations during the period from 2004 to 2010. Although the ACE-FTS never observes true nighttime conditions, it does observe Antarctic twilight [NO] in the MLT over a similar time span to the Odin time series. Due to the long lifetime of NO in this region, on the order of hours, the Odin-ACE comparisons are useful for measuring weekly to year-to-year [NO] variations. As a further check, the satellite-derived [NO] data are also compared with simulated nighttime [NO] from the Specified Dynamics-Whole Atmosphere Community Climate Model (SD-WACCM).

[7] The satellite-derived data, associated retrieval methods, and model data are described in section 2. Section 3 presents the results of comparisons between OSIRIS, SMR, ACE-FTS, and SD-WACCM three-day running mean, vertically averaged [NO], and their relation to variations in solar activity. Direct comparisons of colocated OSIRIS/SMR profiles are also presented, as well as the [NO] climatologies derived from the Odin and SD-WACCM data sets. The results are summarized and discussed in section 4.

2. Description of the [NO] Data Sets and Satellite Instruments

[8] The Odin satellite was launched into a sun-synchronous orbit in February 2001 [*Murtagh et al*., 2002]. On board are two separate instruments, OSIRIS [*Llewellyn et al*., 2004] and SMR [*Frisk et al*., 2003], which have coaligned lines of sight and scan the Earth's limb between tangent heights from approximately 7 to 115 km. The Odin orbit has a nominal ascending (descending) node near 06:00 LT (18:00 LT), and due to the orbital geometry Odin only observes true nighttime conditions (tangent point solar zenith angles greater than 102°) in the Southern high latitudes between April and August, inclusive. However, the OSIRIS and SMR sampling of NO in the MLT have been on separate schedules over the course of the Odin mission. Until early 2007, OSIRIS only took measurements in the MLT for approximately one day out of every 10 days, while the SMR would measure [NO] in the MLT for approximately one day out of 30. Starting on April 2007, OSIRIS increased MLT sampling to every other day, and the SMR sampling of [NO] increased to at least one out of every 10 days.

[9] The OSIRIS optical spectrograph observes scattered sunlight and airglow emission in the near ultraviolet to near infrared, from 275 to 810 nm, with an approximately 1 nm spectral resolution. The optical spectrograph has an approximate 1 km vertical resolution, and measurements are typically vertically separated by 1.5 km. The OSIRIS [NO] retrieval technique, discussed in more detail by *Gattinger et al*. [2009, 2010] and *Sheese et al*. [2011a], fits a model spectrum [*Becker et al*., 1972] to the OSIRIS observations of the NO_2 afterglow continuum over the wavelength range 430–810 nm in order to determine the limb radiance profiles. The definitive measurement of the NO_2 afterglow spectral profile made by *Becker et al*. [1972] remains unchallenged, as the reaction vessel they used was unique, being 7.5 m in diameter. They clearly observed a shift of the NO_2 continuum spectral peak with vessel pressure, an effect included in the spectral fitting analysis used in this study. In this study, a modeled OH airglow spectrum is subtracted from the total observed spectrum to isolate the continuum component. The spectral shape of the laboratory spectrum is fit to bright OSIRIS spectra over the 380–810 nm range.

[10] Continuum limb radiance profiles are inverted to determine NO_2 afterglow volume emission rate (VER) profiles, which are used to retrieve [NO] profiles using simultaneously derived OSIRIS temperature and [O] profile retrievals [*Sheese et al*., 2010, 2011b]. The retrieved [O] profiles are limited to an altitude range of approximately 85–100 km, and therefore the [NO] profiles are likewise limited to an altitude range of 85–100 km. A test on the OSIRIS [NO] data set was performed in order to determine the effect of using the OSIRIS-derived temperatures as opposed to climatological temperature profiles, obtained from the NRL-MSIS-E-00 model [*Picone et al*., 2002]. The effect on the Antarctic zonal mean profile was less than 10% in the altitude range of 88–97km, less than 20% at higher altitudes, and less than 30% at lower altitudes. The vertical distribution of the mean NO profile is not significantly changed by substituting OSIRIS temperatures with climatological values from MSIS. The systematic and mean random uncertainty profiles are shown in Figure 1. The systematic uncertainties assume

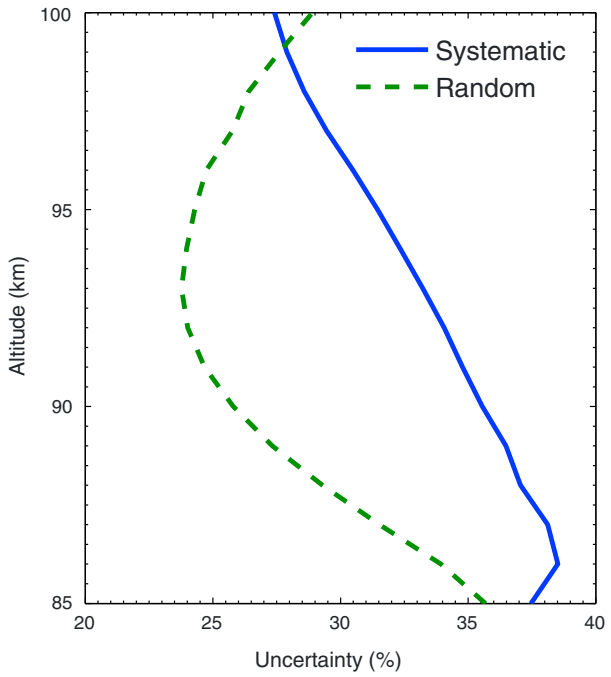

Figure 1. Systematic uncertainty and mean random uncertainty due to instrument noise in the OSIRIS [NO] profiles.

10% systematic uncertainty in both the background density (obtained from MSIS) and temperature profiles, 30% systematic uncertainty in the OSIRIS [O] profile, and 15% uncertainty in both the two-body and three-body reaction coefficients. Systematic uncertainties due to OH airglow removal when fitting to the continuum are assumed to be insignificant in this region. The random uncertainty is due to instrument noise propagated through the VER retrievals. The systematic uncertainties are greatest, ~38%, at 86 km and decrease with altitude to ~28% at 100 km. The mean random uncertainty is lowest, ~24%, at 93 km, and greatest, ~36%, at 85 km.

[11] The SMR observes NO thermal emission lines in a band centered near 551.7 GHz and uses an optimal estimation technique to derive NO volume mixing ratios (VMR) from the observations. SMR level 2, version 2.1 NO data were used in this study, for which the retrieval vertical resolution is ~7 km in the MLT. SMR measurements are consistently made on a ~3 km grid, but the NO retrievals in the MLT are made on a ~5 km grid. Profiles are then linearly interpolated onto a 1 km grid and converted from NO VMR to [NO] using the SMR temperature and pressure profiles, which are from COSPAR international reference atmosphere (CIRA) climatology. Unfortunately, neither SMR nor OSIRIS is currently retrieving pressure or background density profiles in the MLT region, and therefore the SMR NO conversion requires climatological background densities. The use of CIRA climatology in the VMR to density conversion introduces a systematic uncertainty of less than 10% into the SMR [NO] data; however, it should be noted that the CIRA climatology is also used in the SMR NO VMR retrieval, and the conversion is therefore internally consistent. The mean retrieval error in the Antarctic night MLT profiles varies little with altitude, in the range of 44–48%. The two major factors contributing to the single-profile noise are the signal-to-noise ratio determined by two relatively weak lines in the observed band and the single-sideband receiver noise temperature of 3000–3500 K; [*Urban et al*., 2007]. Only values where the measurement response (a measure of the relative contributions of the measurements and the a priori to the retrieved profile [*Rodgers*, 2000]) was greater than 0.75 were considered in the analysis, and this led to a rejection of ~6% of the SMR data. As the SMR NO VMR retrieval is performed on a logarithmic scale, a positive bias may be introduced in regions of low NO VMR. In the auroral regions, this bias is typically only significant near and below altitudes of ~85 km.

[12] A full analysis of the uncertainties associated with the SMR NO data has not been performed; however, common causes of systematic errors within the 551.7 GHz band are known and have previously been quantified. Both pointing errors and uncertainties of the antenna pattern are small compared to the vertical resolution of the NO measurements [*Urban et al*., 2007]. Spectroscopic errors are assumed to be small as the line-broadening parameters for the NO transitions have been measured in the laboratory to an accuracy within ~3% [*Colmont et al*., 2001]. Other spectroscopic parameters are typically known to higher accuracy or lead to smaller uncertainties. Additive calibration errors are estimated to be insignificant as NO is retrieved from the line contrast (background is near zero Kelvin at lower thermospheric altitudes). Multiplicative calibration errors are estimated to be within 2% [*Urban et al*., 2005]. An uncertainty in the sideband ratio also leads to a multiplicative error, which is estimated to be on the order of 3–6% for the 551.7 GHz band [*Eriksson and Urban*, 2009].

[13] The ACE satellite was launched into a circular polar orbit in August 2003 [*Bernath et al*., 2005]. Since the ACE-FTS is a solar occultation instrument, it is limited to twilight conditions and scans the Earth's limb only twice each orbit, with a vertical resolution of ~4 km. ACE-FTS level 2, version 2.2 NO data were used in the analyses, interpolated onto a 1 km grid. For derivations of NO VMR, the ACE-FTS retrieval algorithm [*Boone et al*., 2005] utilizes 20 microwindows within the NO fundamental band region from 1842.9 to 1923.5 cm^{-1}. NO VMR profiles are converted to [NO] using ACE-FTS-derived temperature and pressure profiles. In the MLT, the ACE-FTS [NO] retrieval is essentially independent of the background density, and therefore there is no uncertainty in the MLT ACE-FTS [NO] due to VMR conversion as long as the conversion is consistent with the background densities used in the retrieval. The ACE-FTS data set does not include any estimates of either systematic or random error, but rather only statistical fitting errors, which represent the 1σ statistical fitting errors in the ACE-FTS nonlinear least squares fitting retrieval. The mean fitting error profile decreases nearly linearly with altitude from 46% at 85 km to 16% at 100 km. Although *Kerzenmacher et al*. [2008] validated the ACE-FTS lower mesospheric NO data product, MLT NO was only compared with ~30 coincident NO profiles derived from HALOE observations. Those results indicated that ACE-FTS NO VMRs were typically higher than those of HALOE by ~40% or less in the altitude region of 93–100 km, and no estimates of ACE-FTS systematic or random uncertainties were discussed.

[14] Due to the difference in their measurement techniques, OSIRIS and ACE never make common-volume

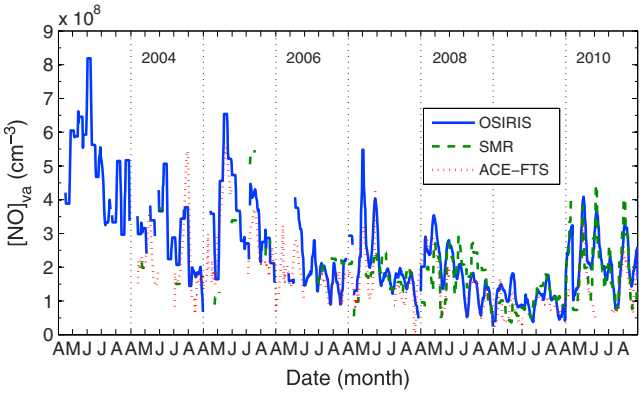

Figure 2. Comparison of OSIRIS, SMR, and ACE-FTS vertically averaged [NO] (vertically averaged between 90 and 100 km) for days 91–244 of each year. Both AM and PM data are included, and data are smoothed by the 10 day running mean.

measurements. However, as the lifetime of NO in the MLT region is on the order of hours-weeks, it is expected that there will be relatively small diurnal variation between twilight and nighttime values at the Odin observation local times. For example, model results from *Bailey et al.* [2002] show that twilight and nighttime [NO] (at mean ACE-FTS and Odin local times) differ by less than 13% at the [NO] peak during fall equinox, and by less than 10% during winter solstice. Although, given different input energy deposition conditions within the model, these values could be significantly different. Ideally, the two data sets would be scaled to a common local time using model simulations of the NO diurnal variation. Model data from two different global climate models (GCMs) were analyzed for this purpose, WACCM and the Thermosphere-Ionosphere-Mesosphere Electrodynamic Global Circulation Model. However, due to large differences between the model results, both in absolute magnitude and spatial and temporal variations, a reliable diurnal variation could not be derived from the simulations, and so no scaling in time has been performed. These differences, along with results from *Bailey et al.* [2002], indicate that in this region differences in [NO] are highly dependent on the auroral input, and currently the best way to accurately simulate energetic particle precipitation (EPP) within a GCM is an open question.

[15] Modeled [NO] profiles were obtained from SD-WACCM, version 4, which constrains the lower atmosphere in the model to meteorological data from the Goddard Earth Observing System 5. The method of nudging lower atmospheric temperature and wind fields within the model are discussed by *Lamarque et al.* [2012, and references therein]. The SD-WACCM model output was chosen for comparison as the model NO simulations are derived in part by auroral forcing, and the auroral forcing within the model is dependent on real K_p planetary geomagnetic index values. As well, as with most GCMs, the gravity wave parameterization is determined in part by lower atmospheric dynamics, and therefore vertical eddy diffusion within SD-WACCM (determined from the gravity wave parameterization) is also influenced by the incorporated meteorological data. NO concentrations in SD-WACCM are determined by the basic middle atmosphere chemistry in the model [*Kinnison et al.*, 2007], by transport, and by ion chemistry, including NO production in the auroral zones. The ion chemistry model within SD-WACCM incorporates ion-neutral, recombination, and photoionization reactions involving electrons, O^+, O_2^+, N^+, N_2^+, and NO^+ [*Marsh et al.*, 2007]. Ionization due to EPP in the auroral regions is parameterized using calculated hemispheric power, which uses K_p index values as an input. In this study, only daily snapshots from the SD-WACCM model, at 0:00 UT, were used. SD-WACCM profiles are provided on pressure levels, and one of the available outputs is geopotential height. The geopotential heights were converted to geophysical altitude using a latitude-dependent Earth radius and were then used to spline-interpolate the SD-WACCM [NO] profiles onto a 1 km altitude grid.

3. Results

[16] All data discussed in this section, unless explicitly stated otherwise, are zonally averaged in the high-latitude region poleward of 60°S, from days 91–244 of the year (April–September), and in the altitude range of 85–100 km. Prior to 2003, OSIRIS was not sampling the atmosphere up to 100 km, and therefore the OSIRIS data set starts in April 2003. In all three data sets, retrieval profiles that contain outliers have been filtered out of the analysis. For all three data sets, outliers for each individual year were determined using the Median Absolute Deviation (MAD) [e.g., *Toohey et al.*, 2010; and references therein]. Due to the large natural variability of the observations, values were determined to be outliers if they were more than 10 times the Median Absolute Deviation ($10 \times$ MAD) greater than the median. In the OSIRIS data, this filtering process flagged less than 6% of the profiles as containing outliers. Both the OSIRIS and ACE-FTS retrievals allow for negative values within the retrieved profile, and negative values were retained in the data sets so as not to skew the mean.

[17] In order to ensure that the SD-WACCM profiles used were truly nighttime conditions, corresponding NO photolysis rate (J_{NO}) profiles were also examined, and only [NO] profiles where all values in the corresponding J_{NO} profile were equal to zero were allowed in the analysis. This sampling leads to a zonal bias, as SD-WACCM snapshots are only available at a single universal time. Although there can be large zonal variations in mesospheric composition, these variations are typically due to planetary wave activity and are averaged out on the timescales over which the SD-WACCM data are being averaged. Additional zonal variation in [NO] density in the Antarctic region occurs due to EPP produced NO (EPP-NO) along the auroral oval [*Sheese et al.*, 2011a], which is not centered over the geographic southern pole. A study is currently underway to sample and analyze SD-WACCM [NO] along the OSIRIS observational path.

3.1. Comparisons of Vertically Averaged [NO]

[18] As is apparent from Figure 2, the mid- to long-term variations exhibited in the OSIRIS, SMR, and ACE-FTS data sets are in reasonable agreement. AM and PM data are included in all three data sets, as OSIRIS observes no significant systematic difference between AM and PM densities, SMR observations exhibit a slight AM positive bias, and the ACE-FTS does not observe Antarctic AM and PM conditions at the same time of the year. All three data sets in Figure 2 have been smoothed by the 10 day running mean

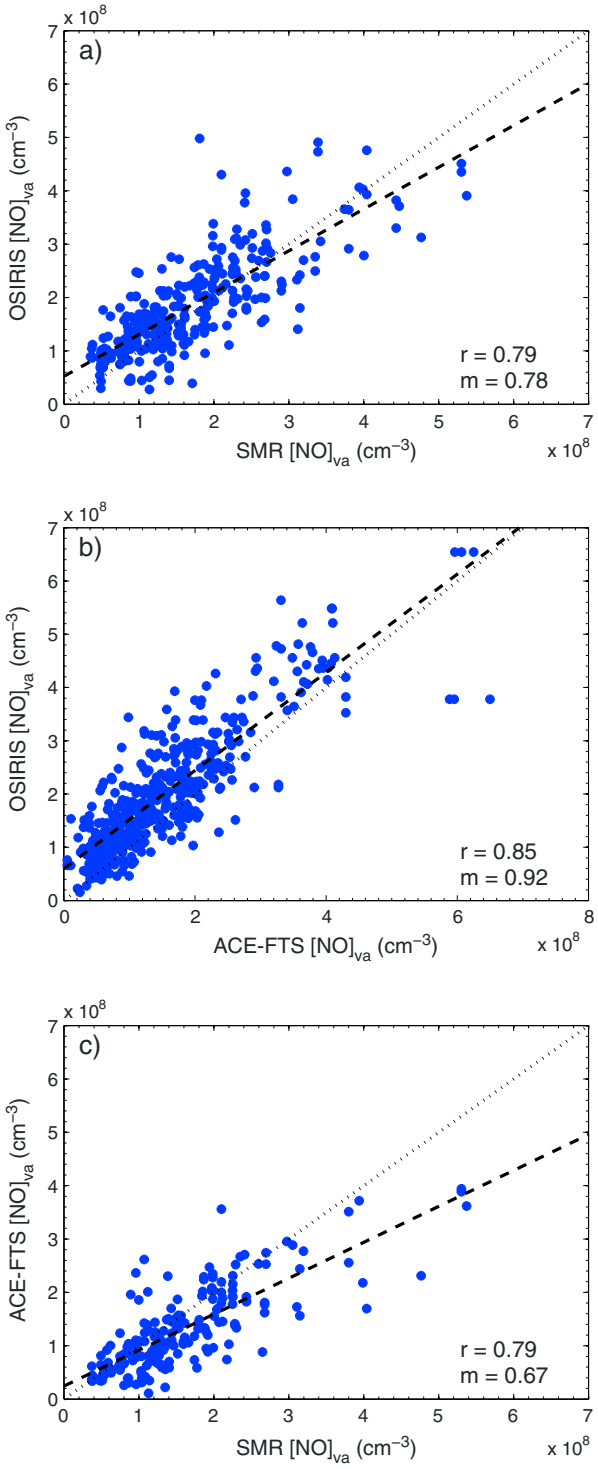

Figure 3. Correlation plots comparing three-day mean $[NO]_{va}$ values between (a) SMR and OSIRIS, (b) ACE-FTS and OSIRIS, and (c) SMR and ACE-FTS. Dashed lines are the linear fits, and dotted lines are the 1-to-1 line. Correlation coefficients, *r*, and slopes of the linear fits, *m*, are also shown.

to reduce noise and highlight variations on monthly timescales. Over the long-term in all three data sets, [NO] vertically averaged between 90 and 100 km (the range over which OSIRIS has the greatest signal-to-noise ratio), $[NO]_{va}$, is observed to decrease during the period from 2003 to 2009, and then begins to increase in 2010. One possible, but unlikely, explanation for this variation in the Odin data is that from 2003 to 2009, the Odin orbit drifted such that both the OSIRIS and SMR observed mean local times at latitudes near 70°S were shifted forward by ~40 min. The Odin orbital drift since 2009 is such that it is now shifting back in the observed local time towards the nominal local time. *Bailey et al*. [2002] modeled [NO] diurnal variations at 65° N for equinox and solstice conditions, both in the presence and absence of auroral activity. For both winter solstice and equinox conditions, the modeled diurnal variations do not exceed 30% from the daily mean and were on the order of 20% in the presence of auroral activity. Given that the lifetime of NO in this region is on the order of hours-weeks, the effect of a shift in local time of only 40 min would not explain the $[NO]_{va}$ decrease of over a factor of 3 that is observed in the OSIRIS data and similarly in the ACE-FTS data, which are not subject to this orbital drift.

[19] However, this variation does correspond well with the 11 year solar cycle. Monthly averaged 2003–2010 OSIRIS $[NO]_{va}$ and corresponding F10.7 solar flux data (obtained from ngdc.noaa.gov) have a correlation coefficient of 0.77. As discussed by *Sheese et al*. [2011a], the OSIRIS data show a relatively strong correlation with the time-shifted A_p index values (a proxy for geomagnetic activity). Lomb-Scargle harmonic analyses [*Press and Rybicki*, 1989] of the vertically averaged OSIRIS $[NO]_{va}$ for 2007–2010, not shown, reveal peak amplitudes each year in the range of 25–29 days. Data prior to 2007 were omitted in this analysis due to the lower OSIRIS mesosphere sampling rate of once every 10 days. These peak amplitudes correspond to the 27 day solar rotation and are at a minimum in 2009 during the prolonged solar minimum between solar cycles 23 and 24.

[20] Three-day running mean $[NO]_{va}$ values of the three data sets show strong correlation with each other, indicating that the variations observed by the three instruments agree well at weekly to annual timescales. Figure 3 shows correlation plots for comparisons of three-day mean $[NO]_{va}$ values. The comparison that yielded the largest correlation coefficient, *r*, is that between OSIRIS and ACE-FTS, where $r = 0.85$. The comparison between OSIRIS and SMR $[NO]_{va}$ yielded a correlation coefficient of $r = 0.79$, and between ACE-FTS and SMR, $r = 0.79$. It should be noted that due to the SMR sampling rate, SMR three-day mean $[NO]_{va}$ values are essentially daily values. Slopes of the linear fits, *m*, are also shown in Figure 3 and are much less than 1 when comparing with SMR. This is, in part, indicative of the systematic differences between the data sets, but is mostly due to the SMR NO concentrations being retrieved on a natural-logarithmic scale, which does not allow for the SMR retrieval to derive negative concentrations.

[21] Comparing 323 OSIRIS and SMR three-day mean $[NO]_{va}$ values, OSIRIS values are on average 10% larger, with a standard deviation of the mean difference of 39%; and a comparison of 452 OSIRIS and ACE-FTS values shows that the OSIRIS values are on average 31% larger, with a standard deviation of the mean difference of 40%. A comparison of 199 SMR and ACE-FTS values shows that SMR values are on average 21% larger, with a standard deviation of the mean difference of 39%. In all three cases, the percent difference values were on the order of or within the

Table 1. Mean Percent Differences in Three-Day Mean $[NO]_{va}$ Between Each Pair of Instruments

Instruments	Mean % Diff.	1 σ (%)	# of Points
OSIRIS-ACE-FTS	31.0	39.5	452
OSIRIS-SMR	10.3	38.7	323
SMR-ACE-FTS	21.0	39.1	199

estimated OSIRIS systematic uncertainties, ~27–36% in this region (90–100 km), and a summary of the percent differences is shown in Table 1. ACE-FTS data are expected to be slightly lower than the other data sets, as NO loss due to photolysis at twilight is a NO sink, even while auroral production of NO is occurring [*Bailey et al.*, 2002]. The majority of the difference between the data sets, however, is most likely due to systematic differences. A difference between ACE-FTS and SMR is also expected as the two density data sets were converted from VMR values by using different background densities. In a comparison of all coincident SMR and ACE-FTS observations, the SMR CIRA climatological background densities in the 90–100 km region were typically 5–10% larger than ACE-FTS derived densities. As previously mentioned, there is no significant uncertainty in ACE-FTS [NO] due to VMR conversion, and the SMR conversion is also internally consistent. Therefore, the difference between SMR and ACE-FTS [NO] due to differences in the background densities is estimated to be less than 10%.

[22] Daily SD-WACCM $[NO]_{va}$ values were determined by vertically averaging all nighttime-condition profiles, as determined by corresponding J_{NO} values, poleward of 60°S between 90 and 100 km, for each daily snapshot. Figure 4a shows this SD-WACCM time series compared with the OSIRIS $[NO]_{va}$ time series seen in Figure 2. The SD-WACCM data have also been smoothed by the 10 day running mean to match those of the three instruments. The SD-WACCM $[NO]_{va}$ values are on the same order as those of OSIRIS, especially at times nearer winter solstice. From April to the beginning of June, OSIRIS and ACE-FTS tend to exhibit greater NO concentrations than SD-WACCM (with the exception of 2009). SMR also exhibits greater NO concentrations than SD-WACCM in April-June 2010; however, the SMR sampling was too sparse prior to 2007 to observe this difference. OSIRIS exhibits slightly greater NO concentrations during August–September 2003–2005 and 2010, although this is not a regular feature seen in either the ACE-FTS or SMR data.

[23] In order to rule out the possibility that the lower SD-WACCM $[NO]_{va}$ values is an effect of the vertical sampling, Figure 4b plots the SD-WACCM $[NO]_{va}$ values along with the daily SD-WACCM 50–130 km NO partial column density values. There is little difference in the variations seen in the partial column density time series compared with those of the $[NO]_{va}$ time series. The low SD-WACCM [NO] is possibly due to low EPP-NO in the SD-WACCM model during

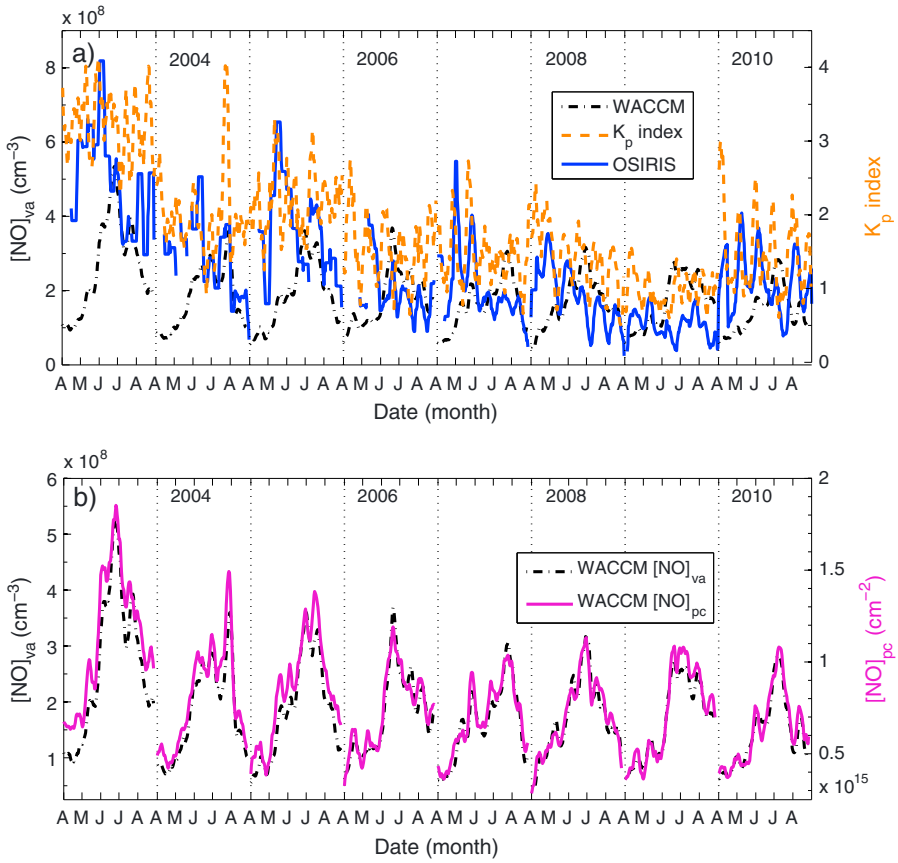

Figure 4. (a) Comparison between OSIRIS (same conditions as Figure 2) and 10 day mean SD-WACCM $[NO]_{va}$ and 10 day averaged 3 h K_p index values. (b) 10 day mean SD-WACCM $[NO]_{va}$ compared with SD-WACCM $[NO]_{pc}$ (partial column densities from 50 to 130 km).

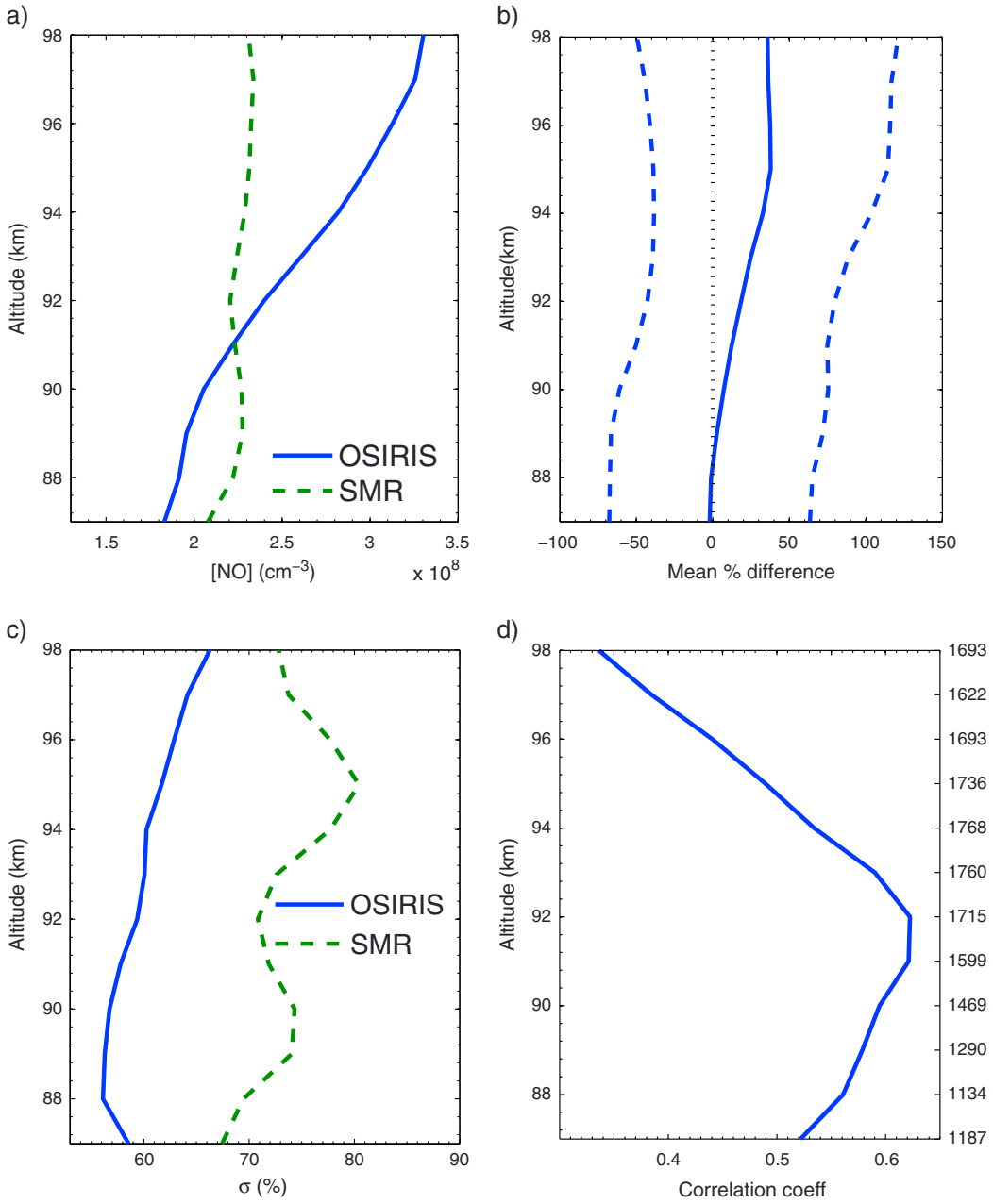

Figure 5. Statistical analysis of coincident OSIRIS and SMR profiles. OSIRIS profiles have been vertically smoothed using the 7 km running mean, and coincident profiles where the OSIRIS values are negative have been excluded. (a) Mean coincident OSIRIS and SMR [NO] profiles. (b) Mean percent difference profiles, 100% (OSIRIS − SMR) / mean, dashed lines indicate the ±1σ standard deviation. (c) OSIRIS and SMR measurement standard deviations. (d) Correlation coefficient profiles. Numbers on right-hand side indicate number of coincident retrievals at a given altitude.

times where there are more sunlit hours in a day. Figure 4a also compares the OSIRIS and SD-WACCM $[NO]_{va}$ time series with 10 day averages of 3 h K_p index values (obtained from ngdc.noaa.gov), which are used as input for SD-WACCM auroral forcing calculations. The OSIRIS time series (which shows strong correlation with the ACE-FTS and SMR time series) exhibits good correlation with the averaged 3 h K_p index values, with a correlation coefficient of 0.74. If time lags are introduced into the K_p index time series, a maximum correlation with the OSIRIS data is achieved with a 4 day lag, with a correlation coefficient of 0.82. This is indicative of NO initially being produced at higher altitudes and being transported into the 90–100 km altitude range; it also indicates that the production of NO is dependent on recent auroral activity, not solely on instantaneous energy deposition [e.g., *Cravens*, 1981]. The SD-WACCM time series also sees a maximum correlation with the K_p time series with a 4 day lag, with a correlation coefficient of only 0.43. Although the

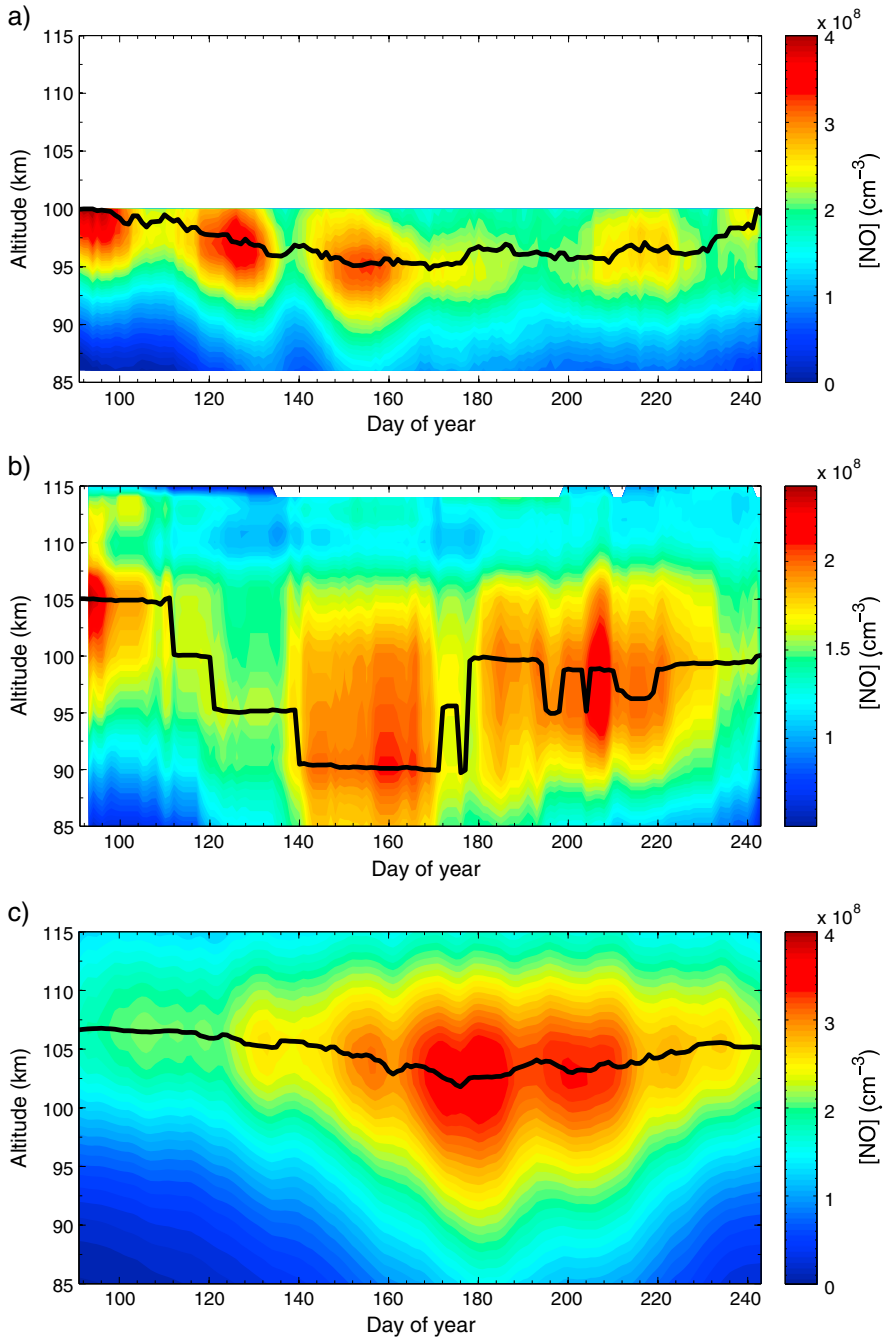

Figure 6. Antarctic [NO] climatologies for 2003–2010 from (a) OSIRIS, (b) SMR, and (c) SD-WACCM. The OSIRIS and SD-WACCM data are smoothed by their respective 10 day running means, whereas the SMR data are smoothed by the 30 day running mean. The solid black lines indicate the [NO] peak altitude.

K_p index is only a moderate proxy of EPP, it is clear that the SD-WACCM NO concentration in this region is not as strongly dependent on EPP as the measurements.

3.2. Comparisons of Odin [NO] Profiles

[24] As OSIRIS and SMR are both on board Odin with colocated lines of sight, near common-volume comparisons can be made between the two data sets. However, as previously mentioned, the two instruments have different sampling rates and vertical resolutions, as well as different horizontal fields of view. In order to compare the two data sets directly, each OSIRIS profile was smoothed with a 7 km running mean in order to match the SMR vertical resolution. Direct comparisons between over 1700 coincident OSIRIS and SMR profiles were made for two different cases—first, all coincident profiles were compared, and then only profile data where the OSIRIS data were positive were compared. The majority of the negative OSIRIS values occur during 2008–2009, when geomagnetic activity was at a minimum.

[25] In both cases, there is little to no agreement in the mean coincident profiles, with OSIRIS exhibiting greater [NO] values than SMR by approximately 20–40% at the

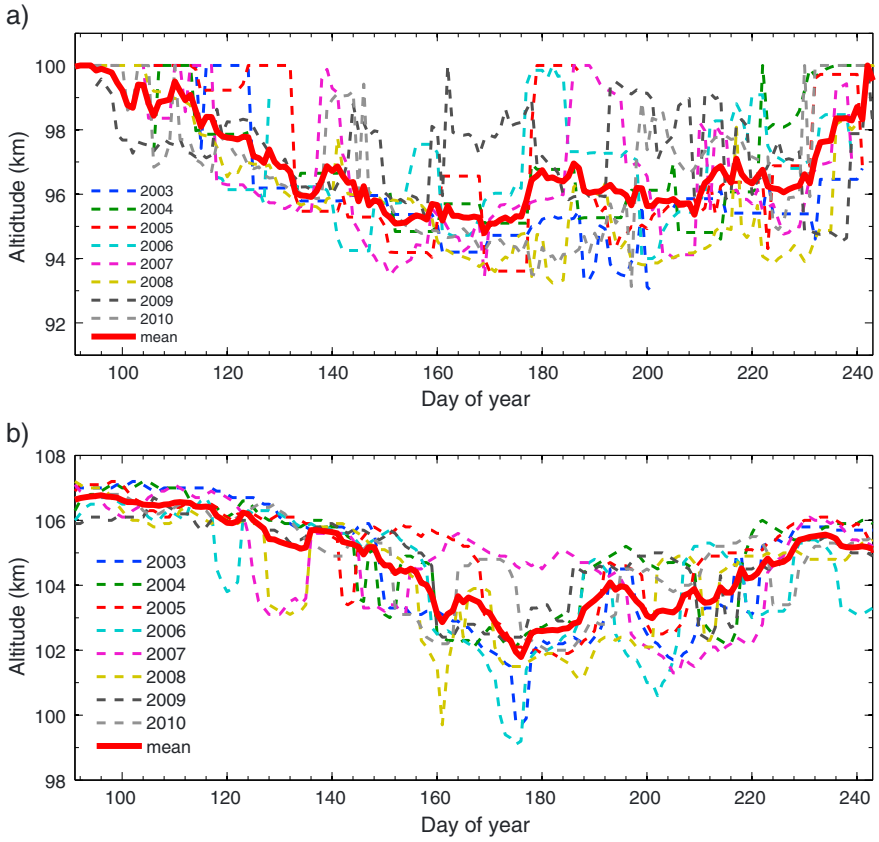

Figure 7. 2003–2010 climatological [NO] peak heights from (a) OSIRIS and (b) SD-WACCM.

higher altitudes, and lower [NO] values than SMR by approximately 15–30% at the lower altitudes. Figure 5a shows the mean OSIRIS and SMR profiles for the case where negative OSIRIS profiles have been excluded. The mean of the percent differences between the individual coincident profiles in this case, shown in Figure 5b, indicates that at altitudes of 90 km and below, OSIRIS values on average are within 8% of the SMR values. At 94 km and above, OSIRIS values are greater than those of SMR by ~35%. These differences do exceed the OSIRIS systematic uncertainties, and the standard deviations of the percent difference profile are large, on the order of 60–80%. Including negative OSIRIS values leads to very large percent difference values, and therefore results for this case are not shown.

[26] Both data sets exhibit large standard deviations, shown in Figure 5c. The SMR values are on the order of 75%, whereas the OSIRIS standard deviations range between 56 and 66%. It should be noted that these values represent both random uncertainty and natural variability, the latter of which is large over the solar cycle. The largest correlation between the two data sets, Figure 5d, is at an altitude of 92 km, with a correlation coefficient of approximately $r = 0.61$. This is significantly lower than the correlation between the OSIRIS and SMR three-day mean $[NO]_{va}$ values; although this is expected, as the $[NO]_{va}$ averages out much of the random error associated with the individual profiles.

[27] Altogether, the poor agreement in the mean coincident OSIRIS and SMR profiles, the large standard deviations, and the poor correlation between the data sets lead the authors to question the validity of the individual profiles of both instruments. Given the lack of other nighttime NO data with which to compare at this time, it is not possible to determine which data set's individual profiles are more reliable. Therefore, the authors note that neither data set's individual profiles have been validated and the data sets can only be used for climatological purposes.

3.3. Profile Climatologies

[28] Previous satellite measurements of [NO] profiles outside of the dark polar region [e.g., *Siskind et al.*, 1998; *Barth et al.*, 2003] have shown that [NO] typically peaks in the 106–110 km region. However, in all three of the satellite-derived data sets analyzed in this study, a different phenomenon is observed. Figure 6 shows profile time series composites of the 2003–2010 OSIRIS, 2004–2010 SMR, and 2003–2010 SD-WACCM [NO] data. ACE-FTS data were not considered in the climatology analysis as ACE-FTS does not observe the dark polar region near winter solstice. The OSIRIS and SD-WACCM data were smoothed with the 10 day running mean in order to reduce noise and to highlight seasonal variations, and the SMR data were smoothed with the 30 day running mean due to SMR's lower sampling rate. The step-function nature of the SMR climatology is due to the SMR 5 km vertical retrieval grid. Although there are significant differences between the OSIRIS and SMR autumn-winter climatologies, both exhibit a [NO] peak height that descends to an altitude below 100 km. At the beginning of autumn, the SMR [NO] maximum is near an altitude of 105 km, close to the accepted [NO] peak height, and the OSIRIS data exhibit a [NO] peak closer to 100 km. However, it is possible that

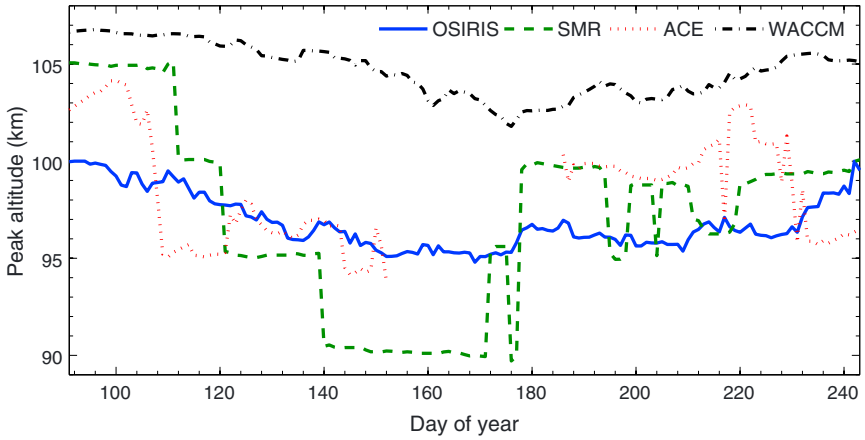

Figure 8. Peak heights of the satellite-derived and modeled NO climatologies. The SMR data were smoothed by the 30 day running mean, and all other data were smoothed by the respective 10 day running means.

the OSIRIS peak height is artificially low at this time due to the fact that 100 km is the highest altitude at which OSIRIS is deriving [NO]. In both the OSIRIS and SMR climatologies, the peak height decreases throughout the autumn to a minimum peak height around winter solstice, and then rises again throughout the rest of the winter to roughly 100 km on day 244. Near winter solstice, the OSIRIS climatological peak height reaches a minimum altitude of ~95 km, whereas the SMR minimum is closer to 90 km. This bias, and the poor agreement in peak height throughout the seasons, could in part be due to the SMR 5 km vertical retrieval grid.

[29] The SD-WACCM climatology shows a somewhat similar variation throughout the autumn-winter, only at higher altitudes. Throughout the autumn, the SD-WACCM climatology exhibits a peak height that descends from 107 km to ~102 km near winter solstice then rises again throughout the winter to ~105 km. Figures 7a and 7b compare the OSIRIS and SD-WACCM peak height descents for individual years from 2003 to 2010. With the possible exceptions of 2009 in the OSIRIS data and 2007 in the SD-WACCM data, this ~5 km vertical descent is observed every year in both data sets.

[30] A 2004–2010 ACE-FTS climatology was also constructed and smoothed by the 10 day running mean, in order to check if there is any evidence of this descent in the twilight data. Figure 8 shows the [NO] peak heights from all three satellite-derived climatologies compared with that of SD-WACCM. The ACE-FTS peak heights do not completely agree with any one data set throughout the entire autumn-winter period, but rather exhibit some agreement with OSIRIS or SMR at different times. At the beginning of autumn, ACE-FTS agrees somewhat with SMR, with peak heights descending from ~104 km. Mid to late autumn, ACE-FTS agrees well with OSIRIS, with peak heights near 96 km, and midwinter, both ACE-FTS and SMR peak heights are near 100 km. Despite the large disagreements between the four data sets, there is agreement that near winter solstice, the Antarctic [NO] peak height decreases significantly from the accepted density peak height of ~106 km.

4. Summary and Discussion

[31] An eight-year OSIRIS data set of Antarctic [NO] in the MLT has been compared with similar data sets from SMR, ACE-FTS, and SD-WACCM. Comparisons of vertically averaged satellite-derived data poleward of 60°S show good agreement in the weekly, monthly, and year-to-year variations. As NO at high latitudes is produced predominantly through auroral precipitation, these variations correspond to changes in solar activity. In all three data sets, $[NO]_{va}$ (NO densities vertically averaged from 90 to 100 km) decrease significantly from the beginning of their time series (2003–2004) to 2009, the solar cycle 23 minimum. $[NO]_{va}$ then increases significantly in 2010 with the onset of solar cycle 24.There is evidence of a ~27 day cycle present in each of the three satellite-derived data sets, and the OSIRIS data set exhibits good correlation, $r = 0.82$, with 4 day lagged daily average 3 h K_p index values. These findings are not a new result, for instance, over two decades ago, *Barth et al.* [1988] linked low-latitude [NO] fluctuations to the solar Lyman-α irradiance 27 day cycle. As well, the SMR and ACE-FTS three-day mean $[NO]_{va}$ values are strongly correlated with those of OSIRIS, with correlation coefficients on the order of 0.8. On average, OSIRIS $[NO]_{va}$ are ~10% larger than SMR values, which is within the OSIRIS systematic errors; and on average, OSIRIS $[NO]_{va}$ are ~30% larger than ACE-FTS values, which is on the same order as the OSIRIS systematic errors and the ACE-FTS fitting errors.

[32] Although there is strong correlation and good agreement between time-averaged $[NO]_{va}$ values of all three data sets, direct comparisons between colocated OSIRIS and SMR [NO] profiles exhibit poor agreement. The mean colocated OSIRIS and SMR profiles show different [NO] vertical distributions, and the absolute mean percent difference between the two is on the order of 35% at altitudes of 94–98 km, but less than 10% below 90 km. Large standard deviations and poor correlations between the colocated profiles indicate that there are large uncertainties associated with individual nighttime OSIRIS and SMR [NO] profiles and therefore should not be used on an individual profile basis. However, the data sets can be useful for investigating long-term [NO] variations and climatology.

[33] Modeled [NO] from SD-WACCM was also compared with the satellite-derived [NO]. The SD-WACCM $[NO]_{va}$ are on the same order as those from OSIRIS, SMR, and ACE-FTS near winter solstice, but are typically much lower than the three satellite-derived data sets from early to mid

autumn. The SD-WACCM $[NO]_{va}$ seasonal variations, which agree with the SD-WACCM 50–130 km partial column density variations, exhibit what would be expected for NO production driven predominantly by solar irradiance, i. e., [NO] is greatest during winter solstice and low near equinox. The strong correlation between the OSIRIS data set and the K_p index values suggests that NO production is much more dependent on auroral activity than solar irradiance throughout the autumn and winter. The seasonal variation of SD-WACCM [NO] and its relatively weak dependence on K_p suggest that the auroral forcing relative to solar irradiance forcing in SD-WACCM is too weak. However, it is possible that SD-WACCM has a strong seasonal cycle in loss rate or in transport that is masking the production variation, and the SD-WACCM zonal sampling bias may also play a minor role in masking the production variation. Further study using the SD-WACCM model with output along the Odin orbital track is needed to determine the sources of this variation.

[34] The autumn-winter climatologies determined from the Odin data sets do exhibit large differences, and further investigation into the Odin NO systematic uncertainties is needed in order to identify the sources of these dissimilarities. However, both data sets exhibit a significant unexpected feature. Nighttime [NO] peak heights descend from near or above 100 km in early autumn to altitudes near 90–95 km around winter solstice. *Sheese et al*. [2011b] have briefly discussed this NO descent, together with a similar decrease in the observed OSIRIS temperatures at all altitudes and a decrease in mesopause height, as being suggestive of net downward advection in the region. The climatology from the SD-WACCM simulations also shows a ~5 km descent in [NO] peak height throughout the autumn, but from an altitude of 107 km down to 102 km. Recent results from WACCM version 3.5 [*Smith et al*., 2011] indicate that at the winter pole, the MLT transitions from downwelling below 90–95 km to upwelling at higher altitudes. *Smith et al*. [2011] also found that transport due to the upward motion at these higher altitudes had little to no effect on the NO VMR vertical distribution. *Lossow et al*. [2009] also discussed similar upwelling seen in WACCM version 3 data for Antarctic winter above 90 km. These results indicate that eddy and molecular diffusion are most likely responsible for the downward transport of NO observed in the OSIRIS, SMR, ACE-FTS, and SD-WACCM data. The difference in absolute altitude between the observed and modeled data is mostly likely due to weak auroral forcing in the SD-WACCM model. More intense EPP will precipitate auroral electrons with greater energies than accounted for in SD-WCACCM, resulting in NO production at lower altitudes. The SD-WACCM model currently does not account for this process, as it is still an open question how to best incorporate this process into GCMs. Further studies are needed to see how this observed feature can be simulated by the models and to determine the exact dynamical and chemical processes responsible.

[35] **Acknowledgments.** This project was funded by grants from the Canadian Space Agency (CSA) and the Natural Sciences and Engineering Research Council Canada (NSERC). Odin is a Swedish-led satellite project funded jointly by Sweden (Swedish National Space Board), Canada (CSA), France (Centre National d'Études Spatiales), and Finland (Tekes), with support by the third party mission program of the European Space Agency (ESA). The Atmospheric Chemistry Experiment is a Canadian-led mission mainly supported by the CSA. The National Center for Atmospheric Research is sponsored by the National Science Foundation. The authors thank the anonymous referees for their valuable comments.

References

Bailey, S. M., C. A. Barth, and S. C. Solomon (2002), A model of nitric oxide in the lower thermosphere, *J. Geophys. Res.*, *107*(A8), 1205, doi:10.1029/2001JA000258.

Barth, C. A. (1964), Rocket measurement of the nitric oxide dayglow, *J. Geophys. Res.*, *69*, 3301–3303, doi:10.1029/JZ069i015p03301.

Barth, C. A., W. K. Tobiska, D. E. Siskind, and D. D. Cleary (1988), Solar-terrestrial coupling: Low-latitude thermospheric nitric oxide, *Geophys. Res. Lett.*, *15*, 92–94, doi:10.1029/GL015i001p00092.

Barth, C. A., K. D. Mankoff, S. M. Bailey, and S. C. Solomon (2003), Global observations of nitric oxide in the thermosphere, *J. Geophys. Res.*, *108*(A1), 1027, doi:10.1029/2002JA009458.

Becker, K. H., W. Groth, and D. Thran (1972), The mechanism of the air afterglow $NO + O \rightarrow NO_2 + hv$, *Chem. Phys. Lett.*, *15*, 215–220, doi:10.1016/0009-2614(72)80152-0.

Bermejo-Pantaleón, D., et al. (2011), Global observations of thermospheric temperature and nitric oxide from MIPAS spectra at 5.3 μm, *J. Geophys. Res.*, *116*, A10313, doi:10.1029/2011JA016752.

Bernath, P. F., et al. (2005), Atmospheric Chemistry Experiment (ACE): Mission overview, *Geophys. Res. Lett.*, *32*, L15S01, doi:10.1029/2005GL022386.

Boone, C. D., R. Nassar, K. A. Walker, Y. Rochon, S. D. McLeod, C. P. Rinsland, and P. F. Bernath (2005), Retrievals for the atmospheric chemistry experiment Fourier-transform spectrometer, *Appl. Opt.*, *44*, 7218–7231, doi:10.1364/AO.44.007218.

Colmont, J.-M., J.-F. D'Eu, F. Rohart, G. Wlodarczak, and J. Buldyreva (2001), N_2- and O_2-Broadenings and Lineshapes of the 551.53-GHz Line of ^{14}NO, *J. Mol. Spectrosc.*, *208*, 197–208, doi:10.1006/jmsp.2001.8381.

Cravens, T. E. (1981), The global distribution of nitric oxide at 200 km, *J. Geophys. Res.*, *86*, 5710–5714, doi:10.1029/JA086iA07p05710.

Eriksson, P., and J. Urban (2009), Post launch characterisation of Odin-SMR sideband filter properties, technical report, Dep. of Radio and Space Sci., Chalmers Univ. of Technol., Gothenburg, Sweden.

Frisk, U., et al. (2003), The Odin satellite. I. Radiometer design and test, *Astron. Astrophys.*, *402*, L27–L34, doi:10.1051/0004-6361:20030335.

Funke, B., M. López-Puertas, S. Gil-López, T. von Clarmann, G. P. Stiller, H. Fischer, and S. Kellmann (2005a), Downward transport of upper atmospheric NO_x into the polar stratosphere and lower mesosphere during the Antarctic 2003 and Arctic 2002/2003 winters, *J. Geophys. Res.*, *110*, D24308, doi:10.1029/2005JD006463.

Funke, B., et al. (2005b), Retrieval of stratospheric NO_x from 5.3 and 6.2 μm nonlocal thermodynamic equilibrium emissions measured by Michelson Interferometer for Passive Atmospheric Sounding (MIPAS) on Envisat, *J. Geophys. Res.*, *110*, D09302, doi:10.1029/2004JD005225.

Gardner, J. L., B. Funke, M. G. Mlynczak, M. López-Puertas, F. J. Martin-Torres, J. M. Russell, S. M. Miller, R. D. Sharma, and J. R. Winick (2007), Comparison of nighttime nitric oxide 5.3 μm emissions in the thermosphere measured by MIPAS and SABER, *J. Geophys. Res.*, *112*, A10301, doi:10.1029/2006JA011984.

Gattinger, R. L., W. F. J. Evans, I. C. McDade, D. A. Degenstein, and E. J. Llewellyn (2009), Observation of the chemiluminescent $NO + O \rightarrow NO_2 + hv$ reaction in the upper mesospheric dark polar regions by OSIRIS on Odin, *Can. J. Phys.*, *87*, 925–932, doi:10.1139/P09-051.

Gattinger, R. L., et al. (2010), NO_2 air afterglow and O and NO densities from Odin-OSIRIS night and ACE-FTS sunset observations in the Antarctic MLT region, *J. Geophys. Res.*, *115*, D12301, doi:10.1029/2009JD013205.

Gordley, L., et al. (1996), Validation of nitric oxide and nitrogen dioxide measurements made by the Halogen Occultation Experiment for UARS platform, *J. Geophys. Res.*, *101*, 10,241–10,266, doi:10.1029/95JD02143.

Kerzenmacher, T., et al. (2008), Validation of NO_2 and NO from the Atmospheric Chemistry Experiment (ACE), *Atmos. Chem. Phys.*, *8*, 5801–5841, doi:10.5194/acp-8-5801-2008.

Kinnison, D. E., et al. (2007), Sensitivity of chemical tracers to meteorological parameters in the MOZART-3 chemical transport model, *J. Geophys. Res.*, *112*, D20302, doi:10.1029/2006JD007879.

Lamarque, J.-F., et al. (2012), CAM-chem: description and evaluation of interactive atmospheric chemistry in the Community Earth System Model, *Geosci. Model Dev.*, *5*, 369–411, doi:10.5194/gmd-5-369-2012.

Llewellyn, E. J., et al. (2004), The OSIRIS instrument on the Odin spacecraft, *Can. J. Phys.*, *82*, 411–422, doi:10.1139/P04-005.

Lossow, S., J. Urban, H. Schmidt, D. R. Marsh, J. Gumbel, P. Eriksson, and D. Murtagh (2009), Wintertime water vapor in the polar upper mesosphere and lower thermosphere: First satellite observations by Odin submillimeter radiometer, *J. Geophys. Res.*, *114*, D10304, doi:10.1029/2008JD011462.

Marsh, D. R., R. R. Garcia, D. E. Kinnison, B. A. Boville, F. Sassi, S. C. Solomon, and K. Matthes (2007), Modeling the whole atmosphere response to solar cycle changes in radiative and geomagnetic forcing, *J. Geophys. Res.*, *112*, D23306, doi:10.1029/2006JD008306.

McPeters, R. D. (1989), Climatology of Nitric Oxide in the Upper Stratosphere, Mesosphere, and Thermosphere: 1979 through 1986, *J. Geophys. Res.*, *94*, 3461–3472, doi:10.1029/JD094iD03p03461.

Mlynczak, M., et al. (2003), The natural thermostat of nitric oxide emission at 5.3 μm in the thermosphere observed during the solar storms of April 2002, *Geophys. Res. Lett.*, *30*(21), 2100, doi:10.1029/2003GL017693.

Mlynczak, M. G., et al. (2005), Energy transport in the thermosphere during the solar storms of April 2002, *J. Geophys. Res.*, *110*, A12S25, doi:10.1029/2005JA011141.

Murtagh, D., et al. (2002), An overview of the Odin atmospheric mission, *Can. J. Phys.*, *80*, 309–319, doi:10.1139/P01-157.

Picone, J. M., A. E. Hedin, D. P. Drob, and A. C. Aikin (2002), NRL-MSISE-00 Empirical Model of the Atmosphere: Statistical Comparisons and Scientific Issues, *J. Geophys. Res.*, *107*(A12), 1468, doi:10.1029/2002JA009430.

Press, W. H., and G. B. Rybicki (1989), Fast Algorithm for Spectral Analysis of Unevenly Sampled Data, *Astrophys. J.*, *338*, 227–280, doi:10.1086/167197.

Randall, C. E., V. L. Harvey, C. S. Singleton, S. M. Bailey, P. F. Bernath, M. Codrescu, H. Nakajima, and J. M. Russell, III (2007), Energetic particle precipitation effects on the Southern Hemisphere stratosphere in 1992–2005, *J. Geophys. Res.*, *112*, D08308, doi:10.1029/2006JD007696

Rodgers, C. D. (2000), *Inverse Methods for Atmospheric Sounding: Theory and Practice. Ser. on Atmos., Oceanic and Planet. Phys.*, vol. *2*, World Sci., Hackensack, N. J.

Sheese, P. E., E. J. Llewellyn, R. L. Gattinger, A. E. Bourassa, D. A. Degenstein, N. D. Lloyd, and I. C. McDade (2010), Temperatures in the upper mesosphere and lower thermosphere from OSIRIS observations of O_2 A-band emission spectra, *Can. J. Phys.*, *88*, 919–925, doi:10.1139/P10-093.

Sheese, P. E., R. L. Gattinger, E. J. Llewellyn, C. D. Boone, and K. Strong (2011a), Nighttime nitric oxide densities in the Southern Hemisphere mesosphere–lower thermosphere, *Geophys. Res. Lett.*, *38*, L15812, doi:10.1029/2011GL048054.

Sheese, P. E., I. C. McDade, R. L. Gattinger, and E. J. Llewellyn (2011b), Atomic oxygen densities retrieved from Optical Spectrograph and Infrared Imaging System observations of O_2 A-band airglow emission in the mesosphere and lower thermosphere, *J. Geophys. Res.*, *116*, D01303, doi:10.1029/2010JD014640.

Siskind, D. E., C. A. Barth, and J. M. Russell, III (1998), A climatology of nitric oxide in the mesosphere and thermosphere, *Adv. Space Res.*, *21*, 1353–1362, doi:10.1016/S0273-1177(97)00743-6.

Smith, A. K., R. R. Garcia, D. R. Marsh, and J. H. Richter (2011), WACCM simulations of the mean circulation and trace species transport in the winter mesosphere, *J. Geophys. Res.*, *116*, D20115, doi:10.1029/2011JD016083.

Solomon, S., P. J. Crutzen, and R. G. Roble (1982), Photochemical coupling between the thermosphere and the lower atmosphere: 1. Odd nitrogen from 50 to 120 km, *J. Geophys. Res.*, *87*, 7206–7220, doi:10.1029/JC087iC09p07206.

Solomon, S. C., C. A. Barth, and S. M. Bailey (1999), Auroral production of nitric oxide measured by the SNOE satellite, *Geophys. Res. Lett.*, *26*, 1259–1262, doi:10.1029/1999GL900235.

Toohey, M., K. Strong, P. F. Bernath, C. D. Boone, K. A. Walker, A. I. Jonsson, and T. G. Shepherd (2010), Validating the reported random errors of ACE-FTS measurements, *J. Geophys. Res.*, *115*, D20304, doi:10.1029/2010JD014185.

Urban, J., et al. (2005), Odin/SMR limb observations of stratospheric trace gases: Level 2 processing of ClO, N_2O, HNO_3, and O_3, *J. Geophys. Res.*, *110*, D14307, doi:10.1029/2004JD005741.

Urban, J., et al. (2007), Global observations of middle atmospheric water vapour by the Odin satellite: An overview, *Planet. Space Sci.*, *55*, 1093–1102, doi:10.1016/j.pss.2006.11.021.